Oversampled Zak-OTFS Receiver With Superimposed Spread Pilot

Vineetha Yogesh and Ananthanarayanan Chockalingam
Department of ECE, Indian Institute of Science, Bangalore 560012

***Abstract*—Zak transform based orthogonal time frequency space (Zak-OTFS) modulation has garnered research interest owing to its robustness in rapidly time-varying channels and attractive properties such as non-fading and predictability. In this work, we consider channel estimation and data detection in a *superimposed spread pilot framework*, which has the advantage of not incurring throughput loss due to pilot overhead, but also has to deal with the problem of interference between pilot and data. In this framework, we investigate over-sampling at the receiver for channel estimation and data detection, which has not been reported so far. To address the increased computational complexity in processing the over-sampled delay-Doppler domain signal, we propose a parallel branch sampling (PBS) receiver architecture that reaps the benefits of over-sampling at low complexity. For this architecture, we derive the maximum likelihood channel estimate and introduce a selection combining algorithm for reliable data detection. To alleviate the pilot-data interference issue, turbo iterations between channel estimation and detection are performed. Extensive simulation results demonstrate that the proposed over-sampling receiver with turbo iterations achieves good mean square error and bit error rate performance.**

***Index Terms*—Zak-OTFS modulation, delay-Doppler domain, over-sampling, superimposed spread pilot, cross-ambiguity.**

I. INTRODUCTION

Orthogonal time frequency space (OTFS) modulation was introduced as a pre- and post-processing scheme over existing multi-carrier (MC) modulation schemes such as orthogonal frequency division multiplexing (OFDM). This variant of OTFS is known as MC-OTFS in literature [1], [2]. Recently, research on Zak transform [3] based OTFS (Zak-OTFS) has gained attention due to its strong formal mathematical foundation [4], structured input-output relation through twisted convolution operation (Table 3 in [5]), and augmented resilience to a larger range of Doppler spreads compared to MC-OTFS (Fig. 18 in [5]). The performance superiority of Zak-OTFS is attributed to its non-fading and predictability properties [4], [5], [6]. This paper deals with channel estimation and detection problems in Zak-OTFS.

For channel estimation purposes, a known pilot signal is transmitted. In the context of Zak-OTFS, the pilot signal can be transmitted by (i) using an entire Zak-OTFS frame dedicated to a pilot symbol (*exclusive pilot frame*) which incurs throughput loss, (ii) embedding data and pilot symbols in the same frame with guard space in between (*embedded pilot frame*) which also incurs throughput loss, and (iii) superimposing a spread pilot symbol on data symbols in the same frame (*superimposed spread pilot frame [7]*) which has the advantage of not incurring throughput loss but has the need to deal with interference between pilot and data. Motivated by its full-throughput advantage, in this paper, we consider the superimposed spread pilot framework. Recognizing the associated pilot-data interference issues in this framework, we seek to alleviate them by exploiting the benefits of oversampling. To motivate this, we note that conventional receiver sampling at the information delay-Doppler (DD) grid points does not capture the sufficient statistics in fractional DD channels and hence finer sampling (i.e., over-sampling) between the grid points can improve performance [8]. Such improvements in the case of MC-OTFS have been reported in [9]- [11]. Our current study investigates oversampling in Zak-OTFS under the challenging superimposed spread pilot framework, which has not been reported so far. Despite being attractive for improving performance, a direct over-sampling approach has the drawback of increased receiver complexity. Our proposed over-sampling approach in this paper addresses this complexity issue through a novel parallel branch sampling (PBS) that samples the delay- and Doppler-shifted versions of the received signal on the conventional sampling grid and reaps over-sampling benefits at low complexity. For the proposed PBS receiver architecture, we derive the maximum-likelihood (ML) channel estimate and introduce a selection combining based detection algorithm. Turbo iterations between channel estimation and data detection are carried out to alleviate the effects of pilot-data interference. Our simulation results show that the proposed over-sampling receiver with turbo iterations achieves good estimation and detection performance.

II. ZAK-OTFS SYSTEM MODEL

MN symbols in the DD domain, $x[k,l]$, $k \in \{0,1,\cdots,M-1\}$, $l \in \{0,1,\cdots,N-1\}$, are transmitted in one Zak-OTFS frame of size $M \times N$, where M and N are the number of delay and Doppler bins, respectively. A discrete quasi-periodic (QP) signal $x_{\text{dd}}[k,l], \forall k,l \in \mathbb{Z}$ is obtained using $x[k,l]$ as $x_{\text{dd}}[k,l] = x[k,l]$ for $k \in \{0,1,\cdots,M-1\}, l \in \{0,1,\cdots,N-1\}$, and $x_{\text{dd}}[k+nM, l+mN] = x_{\text{dd}}[k,l]e^{j2\pi\frac{nl}{N}}, \forall m,n \in \mathbb{Z}$. The discrete QP DD signal $x_{\text{dd}}[k,l]$ is converted to a continuous QP signal in the DD domain as $x_{\text{dd}}(\tau,\nu) = \sum_{k,l\in\mathbb{Z}} x_{\text{dd}}[k,l]\delta(\tau - k\Delta\tau)\delta(\nu - l\Delta\nu)$, where $\Delta\tau = \frac{\tau_p}{M}$ and $\Delta\nu = \frac{\nu_p}{N}$ are the delay and Doppler resolutions, respectively, and τ_p and ν_p are the delay period and Doppler period, respectively, such that $\tau_p\nu_p = 1$. The fundamental DD grid is defined as $\Lambda_{\text{dd}} = \big\{ (k\Delta\tau, l\Delta\nu) \,\big|\, k = \{0,\cdots,M-1\}, l = \{0,\cdots,N-1\}\big\}$. Note that $x_{\text{dd}}(\tau,\nu)$ is a signal of infinite bandwidth and time. Hence, to restrict its bandwidth and time, it is filtered through a DD domain

This work was supported in part by the J. C. Bose National Fellowship and the NSF-DST project (International Cooperation Division), Department of Science and Technology, Government of India.

$x[k,l]$ is QP if $x[k+nM, l+mN] = x[k,l]e^{j2\pi\frac{nl}{N}}\ \forall\ m,n \in \mathbb{Z}$.

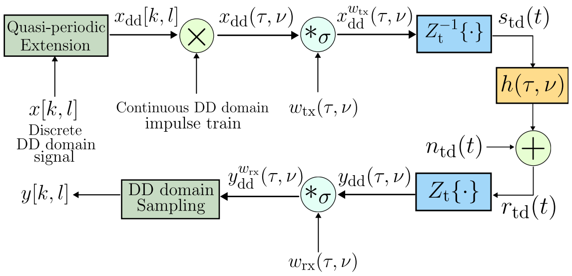

Fig. 1: Block diagram of Zak-OTFS transceiver.

filter $w_{\text{tx}}(\tau,\nu)$ resulting in $x_{\text{dd}}^{w_{\text{tx}}}(\tau,\nu) = w_{\text{tx}}(\tau,\nu) *_\sigma x_{\text{dd}}(\tau,\nu)$, where $*_\sigma$ denotes twisted convolution operation. Note that twisted convolution operation preserves QP. Hence, $x_{\text{dd}}^{w_{\text{tx}}}(\tau,\nu)$ is QP, i.e., $x_{\text{dd}}(\tau+n\tau_p,\nu+m\nu_p) = x_{\text{dd}}(\tau,\nu)e^{j2\pi n\tau_p\nu}$. Finally, $x_{\text{dd}}^{w_{\text{tx}}}(\tau,\nu)$ is converted to time domain using inverse time Zak transform, resulting in the transmit time domain (TD) signal $s_{\text{td}}(t)$ having bandwidth $B \approx M\nu_p$ and time $T \approx N\tau_p$.

The transmitted signal passes through a doubly-selective channel having P paths whose DD domain impulse response is $h(\tau,\nu) = \sum_{i=1}^{P} h_i\delta(\tau-\tau_i)\delta(\nu-\nu_i)$, where h_i, τ_i, and ν_i are the channel gain, delay, and Doppler of the ith path, respectively. The received TD signal is $r_{\text{td}}(t) = \iint h(\tau,\nu)s_{\text{td}}(t-\tau)e^{j2\pi\nu(t-\tau)}d\tau d\nu + n(t)$, where $n(t)$ is the additive white Gaussian noise with one-sided power spectral density N_0. Zak transform is applied on $r_{\text{td}}(t)$ to convert it to DD domain as $y_{\text{dd}}(\tau,\nu) = \mathcal{Z}_t(r_{\text{td}}(t))$. Next, $y_{\text{dd}}(\tau,\nu)$ is filtered through the Rx DD domain filter $w_{\text{rx}}(\tau,\nu)$, which is matched to the Tx DD filter, i.e., $w_{\text{rx}}(\tau,\nu) = w_{\text{tx}}^*(-\tau,-\nu)e^{j2\pi\tau\nu}$. The output of the Rx DD filter is given by $y_{\text{dd}}^{w_{\text{rx}}}(\tau,\nu) = w_{\text{rx}}(\tau,\nu) *_\sigma y_{\text{dd}}(\tau,\nu) = h_{\text{dd}}(\tau,\nu) *_\sigma x_{\text{dd}}(\tau,\nu) + n_{\text{dd}}^{w_{\text{rx}}}(\tau,\nu)$, where $h_{\text{dd}}(\tau,\nu)$ is the effective continuous DD channel, given by $h_{\text{dd}}(\tau,\nu) = w_{\text{rx}}(\tau,\nu) *_\sigma h(\tau,\nu) *_\sigma w_{\text{tx}}(\tau,\nu)$ and $n_{\text{dd}}^{w_{\text{rx}}}(\tau,\nu) = w_{\text{rx}}(\tau,\nu) *_\sigma n_{\text{dd}}(\tau,\nu)$ is the filtered noise in the DD domain and $n_{\text{dd}}(\tau,\nu) = \mathcal{Z}_t(n(t))$. Simplifying $y_{\text{dd}}^{w_{\text{rx}}}(\tau,\nu)$ using the definition of twisted convolution (see footnote 2) and QP property of $x_{\text{dd}}(\tau,\nu)$, we get

$$y_{\text{dd}}^{w_{\text{rx}}}(\tau,\nu) = \sum_{k,l\in\mathbb{Z}} x_{\text{dd}}[k,l]h_{\text{dd}}(\tau-k\Delta\tau,\nu-l\Delta\nu)e^{j2\pi(\nu-l\Delta\nu)k\Delta\tau} + n_{\text{dd}}^{w_{\text{rx}}}(\tau,\nu), \tag{1}$$

Note that $y_{\text{dd}}^{w_{\text{rx}}}(\tau,\nu)$ is QP. Hence, it suffices to obtain its samples within the fundamental period $\tau_p \times \nu_p$, which is further used for receiver processing. The block diagram of the Zak-OTFS transceiver is shown in Fig. 1. In this paper, we consider the signal $x_{\text{dd}}[k,l]$ at the transmitter to be a superposition of data signal (carrying information symbols) and a spread pilot signal (for channel estimation) in the same frame, generated as described below.

A. Superimposed spread pilot signal

The superposition of data and spread pilot is given by

$$x[k,l] = \sqrt{E_{\text{p}}}x_{\text{sp}}[k,l] + \sqrt{E_{\text{d}}}x_{\text{d}}[k,l], \tag{2}$$

where $k \in \{0,1,\cdots,M-1\}, l \in \{0,1,\cdots,N-1\}$, $x_{\text{sp}}[k,l]$ and $x_{\text{d}}[k,l]$ denote the spread pilot and data signals, respectively, and E_{p} and E_{d} denote the average pilot signal energy and data signal energy, respectively, with pilot-to-data power ratio defined as PDR $= \frac{E_{\text{p}}}{E_{\text{d}}}$.

***Data signal*:** Information symbols from a normalized unit energy constellation alphabet $\mathbb{A}$ are embedded on Λ_{dd} to obtain the data signal, i.e., $x_{\text{d}}[k,l] = s, s \in \mathbb{A}$.

***Spread pilot signal*:** A unit energy point pilot at $(k_{\text{p}}, l_{\text{p}})$, defined as $x_{\text{pp}}[k,l] = 1$ for $(k,l) = (k_{\text{p}}, l_{\text{p}})$ and zero otherwise, is filtered through a discrete DD domain filter $w_{\text{s}}[k,l]$ in order to uniformly distribute its energy across the DD grid. The resultant spread pilot signal is obtained as [7]

$$x_{\text{sp}}[k,l] = w_{\text{s}}[k,l] *_\sigma x_{\text{pp}}[k,l] = w[k,l] \circledast_\sigma x_{\text{pp}}[k,l], \tag{3}$$

where $*_\sigma$ denotes discrete domain twisted convolution, $\circledast_\sigma$ is periodic twisted convolution, and $w[k+nMN, l+mMN] = w_{\text{s}}[k,l]$ is the MN periodic extension of $w_{\text{s}}[k,l]$. We use a discrete chirp filter to spread the pilot pilot energy uniformly across the DD bins and the MN-periodic discrete chirp filter is given by [7]

$$w[k,l] = \frac{1}{MN}e^{j2\pi q\frac{(k^2+l^2)}{MN}}, \tag{4}$$

where $k,l \in \mathbb{Z}$ and q is the slope factor. The factor $\frac{1}{MN}$ ensures that the resultant spread pilot signal has unit energy.

B. Receiver over-sampling

The filtered DD domain signal at the receiver given by (1) is directly sampled on the over-sampling grid defined by $\Lambda_{\text{dos}} = \left\{\left(k'\frac{\Delta\tau}{Q_\tau}, l'\frac{\Delta\nu}{Q_\nu}\right) \middle| k' = \{0,1,\ldots,MQ_\tau-1\}, l' = \{0,1,\ldots,NQ_\nu-1\}\right\}$, where Q_τ and Q_ν are over-sampling factors along delay and Doppler domain, respectively ($Q_\tau = Q_\nu = 1$ denotes conventional sampling on Λ_{dd}). The sampled signal can be written in matrix-vector form as

$$\mathbf{y}_{\text{dos}} = \mathbf{H}_{\text{dos}}\mathbf{x} + \mathbf{n}_{\text{dos}}, \tag{6}$$

$\mathbf{y}_{\text{dos}}[k'NQ_\nu + l'] = y_{\text{dd}}^{w_{\text{rx}}}(k'\frac{\Delta\tau}{Q_\tau}, l'\frac{\Delta\nu}{Q_\nu})$, $\mathbf{x}[kN+l] = x[k,l]$, $\mathbf{H}_{\text{dos}}[k'NQ_\nu + l', kN+l]$ is given by (5), and $\mathbf{n}_{\text{dos}}[k'NQ_\nu + l'] = n_{\text{dd}}^{w_{\text{rx}}}(k'\frac{\Delta\tau}{Q_\tau}, l'\frac{\Delta\nu}{Q_\nu})$, with $k \in \{0,1,\cdots,M-1\}, l \in \{0,1,\cdots,N-1\}$. Let $\mathbf{Y}_{\text{dos}}[k,l] = \mathbf{y}_{\text{dos}}[kNQ_\nu + l]$ denote the $MQ_\tau \times NQ_\nu$ received over-sampled matrix.

The size of $\mathbf{Y}_{\text{dos}}$ grows with increase in Q_τ and Q_ν, leading to increased processing complexity. In order to mitigate the increase in complexity, we propose to partition $\mathbf{Y}_{\text{dos}}$ into $Q_\tau Q_\nu$ blocks (each of size $M \times N$) which are used for processing at reduced complexity compared to processing $\mathbf{Y}_{\text{dos}}$ as a whole. Let $\mathbf{Y}_{\text{pbs}}^{(q_\tau+Q_\tau q_\nu)}$ denote the $(q_\tau + Q_\tau q_\nu)$th

$x(\tau,\nu) *_\sigma y(\tau,\nu) = \iint x(\tau',\nu')y(\tau-\tau',\nu-\nu')e^{j2\pi(\tau-\tau')\nu'}d\tau' d\nu'$.

$x(t) = Z_t^{-1}(x(\tau,\nu)) = \sqrt{\tau_p}\int_0^{\nu_p} x(t,\nu)d\nu$.

$x(\tau,\nu) = Z_{\text{t}}(x(t)) = \sqrt{\tau_p}\sum_{k\in\mathbb{Z}} x(\tau+k\tau_p)e^{-j2\pi k\nu\tau_p}$

$a[k,l] *_\sigma b[k,l] = \sum_{k',l'\in\mathbb{Z}} a[k',l']b[k-k',l-l']e^{j2\pi\frac{(k'-k)l'}{MN}}$.

$a[k,l] \circledast_\sigma b[k,l] = \sum_{k'=0}^{MN-1}\sum_{l'=0}^{MN-1} a[k',l']b[k-k',l-l']e^{j2\pi\frac{l'(k-k')}{MN}}$.

With LMMSE equalizer, the DOS system has a detection complexity of $\mathcal{O}(Q_\tau^3 Q_\nu^3 M^3 N^3)$, while with partitioning it reduces to $Q_\tau Q_\nu \mathcal{O}(M^3N^3)$.

$$\mathbf{H}_{\rm dos}[k'NQ_\nu + l', kN + l] = \sum_{m,n\in\mathbb{Z}} h_{\rm dd}\left(k'\frac{\Delta\tau}{Q_\tau} - (k+nM)\Delta\tau, l'\frac{\Delta\nu}{Q_\nu} - (l+mN)\Delta\nu\right) e^{j2\pi\frac{(l'-(l+mN)Q_\nu)(k+nM)}{MNQ_\nu}} e^{j2\pi\frac{nl}{N}}. \quad (5)$$

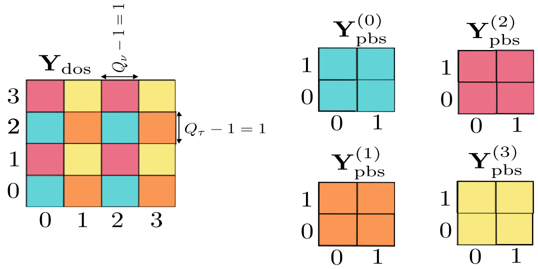

Fig. 2: DOS in the DD domain and partitioning $\mathbf{Y}_{\rm dos}$ matrix into multiple $\mathbf{Y}_{\rm pbs}$ matrices.

partitioned block of size $M \times N$ for a given q_τ and q_ν, where $q_\tau \in \{0, \ldots, Q_\tau - 1\}$ and $q_\nu \in \{0, \ldots, Q_\nu - 1\}$, given by

$$\begin{aligned}\mathbf{Y}_{\rm pbs}^{(q_\tau + Q_\tau q_\nu)} &= \mathbf{Y}_{\rm dos}[q_\tau : Q_\tau : MQ_\tau - Q_\tau + q_\tau, \\ &\quad q_\nu : Q_\nu : NQ_\nu - Q_\nu + q_\nu], \end{aligned} \quad (7)$$

where $[a : c : b] = \{a + sc \mid s = 0, 1, 2, \ldots$ and $a + sc \leq b\}$. Figure 2 illustrates the proposed partitioning for a system with $M = N = 2$ and $Q_\tau = Q_\nu = 2$. $\mathbf{Y}_{\rm dos}$ matrix of size $MQ_\tau \times NQ_\nu$ (i.e., 4×4 matrix in this case) is partitioned into $Q_\tau Q_\nu$ number of $\mathbf{Y}_{\rm pbs}$ matrices each of size $M \times N$ (i.e., 4 matrices, each of size 2×2) as per (7).

III. Proposed parallel branch sampling

The partitioning described above is equivalent to performing conventional sampling on parallel branches where input to each branch is delay- and Doppler-shifted $y_{\rm dd}^{w_{\rm rx}}(\tau, \nu)$ with a delay resolution of $\Delta\tau$ and a Doppler resolution of $\Delta\nu$. The input to the $q' = q_\tau + Q_\tau q_\nu$th branch, $q' \in \{0, \ldots, Q_\tau Q_\nu - 1\}$, is $y_{\rm dd}^{w_{\rm rx}}(\tau + \frac{q_\tau}{Q_\tau}\Delta\tau, \nu + \frac{q_\nu}{Q_\nu}\Delta\nu)$. The sampling instants along delay and Doppler axis are thus $(k' + \frac{q_\tau}{Q_\tau})\Delta\tau$ and $(l' + \frac{q_\nu}{Q_\nu})\Delta\nu$, respectively, where $k' = \{0, \ldots, M-1\}$ and $l' = \{0, \ldots, N-1\}$. The sampled signal on q'th branch by sampling on $\Lambda_{\rm dd}$ is given by (see (1))

$$\begin{aligned} y^{(q')}[k', l'] &= \sum_{k\in\mathbb{Z}}\sum_{l\in\mathbb{Z}} x[k,l] e^{j2\pi\frac{(l'-l)k + \frac{q_\nu}{Q_\nu}k}{MN}} \\ &\quad h_{\rm dd}\left(\left(k' - k + \frac{q_\tau}{Q_\tau}\right)\Delta\tau, \left(l' - l + \frac{q_\nu}{Q_\nu}\right)\Delta\nu\right) + n^{(q')}[k', l'], \\ &\overset{(a)}{=} e^{j2\pi\frac{q_\nu k'}{MNQ_\nu}} \sum_{k''\in\mathbb{Z}}\sum_{l''\in\mathbb{Z}} \tilde{h}^{(q')}[k'', l''] \\ &\quad x_{\rm dd}[k' - k'', l' - l''] e^{j2\pi\frac{l''(k'-k'')}{MN}} + n^{(q')}[k', l'] \\ &= e^{j2\pi\frac{q_\nu k'}{MNQ_\nu}} \left(\tilde{h}^{(q')}[k', l'] *_\sigma x[k', l']\right) + n^{(q')}[k', l'], \end{aligned} \quad (8)$$

where $k'' = k' - k$, $l'' = l' - l$ is used in step (a), $y^{(q')}[k', l'] = y_{\rm dd}^{w_{\rm rx}}\left((k' + \frac{q_\tau}{Q_\tau})\Delta\tau, (l' + \frac{q_\tau}{Q_\tau})\Delta\nu\right)$, $n^{(q')}[k', l'] = n_{\rm dd}^{w_{\rm rx}}\left((k' + \frac{q_\tau}{Q_\tau})\Delta\tau, (l' + \frac{q_\tau}{Q_\tau})\Delta\nu\right)$, $\tilde{h}^{(q')}[k', l'] = h_{\rm dd}\left(\left(k' + \frac{q_\tau}{Q_\tau}\right)\Delta\tau, \left(l' + \frac{q_\nu}{Q_\nu}\right)\Delta\nu\right) e^{-j2\pi\frac{q_\nu k'}{MNQ_\nu}}$, and the samples can be expressed in matrix-vector form as

$$\mathbf{y}^{(q')} = \mathbf{H}^{(q')}\mathbf{x} + \mathbf{n}^{(q')}, \quad (9)$$

where $\mathbf{y}^{(q')} \in \mathbb{C}^{MN\times 1}, \mathbf{x} \in \mathbb{C}^{MN\times 1}$, $\mathbf{H}^{(q')} \in \mathbb{C}^{MN\times MN}$, and $\mathbf{n}^{(q')} \in \mathbb{C}^{MN\times 1}$, such that $\mathbf{x}[kN + l] = x[k, l]$, $\mathbf{H}^{(q')}[k'N + l', kN + l]$ is given by (10) at the top of next page, $\mathbf{n}^{(q')}[kN + l] = n^{(q')}[k, l]$ is the noise, and $\mathbf{y}^{(q')}[k'N + l'] = y^{(q')}[k', l']$. Let $\mathbf{Y}^{(q')}$ denote the $M \times N$ matrix corresponding to the q'th branch constructed such that $\mathbf{Y}^{(q')}[k, l] = \mathbf{y}^{(q')}[kN + l]$.

IV. Proposed algorithms for channel estimation and detection

In this section, we present the proposed channel estimation and detection algorithms for the parallel branch sampling architecture using $\{\mathbf{y}^{(q')}\}_{q'=0}^{Q_\tau Q_\nu - 1}$ and $\{\mathbf{Y}^{(q')}\}_{q'=0}^{Q_\tau Q_\nu - 1}$.

A. Channel estimation using spread pilot

The ML estimate of $h^{(q')}[k, l]$ on q'th branch, denoted by $\hat{\tilde{h}}^{(q')}[k, l]$ is obtained by maximizing the likelihood of observing $y_{\rm sp}^{(q')}[k, l]$ given $\tilde{h}^{(q')}[k, l]$, i.e.,

$$\begin{aligned} \hat{\tilde{h}}^{(q')}[k, l] &= \underset{\tilde{h}^{(q')}[k,l]}{\arg\max}\ \mathrm{P}\left(y_{\rm sp}^{(q')}[k, l] \mid \tilde{h}^{(q')}[k, l]\right) \\ &= \underset{\tilde{h}^{(q')}[k,l]}{\arg\min} \sum_{k=0}^{M-1}\sum_{l=0}^{N-1}\left| y_{\rm sp}^{(q')}[k, l] - e^{j2\pi\frac{q_\nu k}{MNQ_\nu}}\left(\tilde{h}^{(q')}[k, l] *_\sigma x_{\rm sp}[k, l]\right)\right|^2 \\ &\overset{(a)}{=} \sum_{k'=0}^{M-1}\sum_{l'=0}^{N-1} y_{\rm sp}^{(q')}[k, l] x_{\rm sp}^*[k - k', l - l'] e^{-j2\pi\frac{(k-k')l'}{MN}} e^{-j2\pi\frac{q_\nu k}{MNQ_\nu}} \\ &= A_{\tilde{y}_{\rm sp}^{(q')}, x_{\rm sp}}[k, l], \end{aligned} \quad (11)$$

where the equation in step (a) is derived in Appendix A, which is further simplified using $\tilde{y}_{\rm sp}^{(q')}[k, l] = y_{\rm sp}^{(q')}[k, l] e^{-j2\pi\frac{q_\nu k}{MNQ_\nu}}$ and the definition of cross-ambiguity to obtain (11).

Note on cross-ambiguity $A_{\tilde{y}_{\rm sp}^{(q')}, x_{\rm sp}}[k, l]$***:*** $A_{\tilde{y}_{\rm sp}^{(q')}, x_{\rm sp}}[k, l]$ is MN-periodic and is equal to the twisted convolution between the effective channel on q'th branch and the self-ambiguity of the transmitted spread pilot (see Appendix B for derivation), i.e.,

$$A_{\tilde{y}_{\rm sp}^{(q')}, x_{\rm sp}}[k, l] = \tilde{h}^{(q')}[k, l] *_\sigma A_{x_{\rm sp}, x_{\rm sp}}[k, l]. \quad (12)$$

The self-ambiguity of the transmitted spread pilot is supported on a twisted lattice $\Lambda_{\rm q}$ with respect to the period lattice $\Lambda_{\rm p} = \{(nM, mN) | n, m \in \mathbb{Z}\}$ on which the data is embedded (see Fig. 3) [7]. For odd primes M and N, and q relative prime to both M and N, the magnitude profile of $A_{x_{\rm sp}, x_{\rm sp}}[k, l]$ is given by [7]

$$|A_{x_{\rm sp}, x_{\rm sp}}[k, l]| = \begin{cases} 1, & [2qk - l]_M = 0, \\ & [k - l\ ((2q)^{-1} - 2q)]_N = 0 \\ 0, & \text{otherwise}, \end{cases} \quad (13)$$

The noise covariance matrix on q'th branch is $\mathbf{R}^{(q')}$ and its $[k_1 N + l_1, k_2 N + l_2]$th element is $\mathbf{R}^{(q')}[k_1 N + l_1, k_2 N + l_2] = \mathbb{E}[n^{(q')}[k_1, l_1] n^{(q')*}[k_2, l_2]]$. In this work, we consider Gaussian-sinc filter [12] designed to have nulls at conventional sampling instants. Hence, $\mathbf{R}^{(q')} \approx \mathbf{I}_{MN}$, where $\mathbf{I}_{MN}$ is an identity matrix of size MN.

Cross-ambiguity between $y[k, l]$ and $x[k, l]$ is defined as $A_{y,x}[k, l] = \sum_{k'=0}^{M-1}\sum_{l'=0}^{N-1} y[k', l'] x[k' - k, l' - l] e^{-j2\pi\frac{(k'-k)l}{MN}}$.

$$\mathbf{H}^{(q')}[k'N+l', kN+l] = \sum_{m,n\in\mathbb{Z}} h_{\mathrm{dd}}\left(\left(k'+\frac{q_\tau}{Q_\tau}-k-nM\right)\Delta\tau, \left(l'+\frac{q_\nu}{Q_\nu}-l-mN\right)\Delta\nu\right) e^{j2\pi\frac{(l'+\frac{q_\nu}{Q_\nu}-(l+mN))(k+nM)}{MN}} e^{j2\pi\frac{nl}{N}}. \tag{10}$$

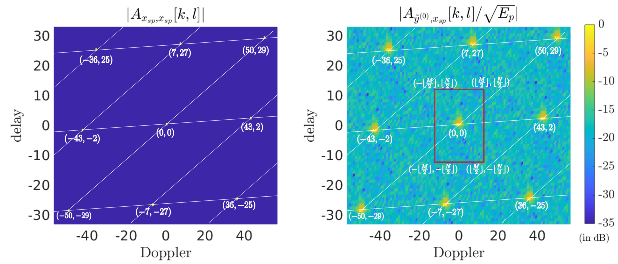

Fig. 3: Heatmap of magnitude (in dB) of $A_{x_{\mathrm{sp}},x_{\mathrm{sp}}}[k,l]$ and $A_{\tilde{y}^{(0)},x_{\mathrm{sp}}}[k,l]/\sqrt{E_{\mathrm{p}}}$ for $M=31, N=37$ system with GS filter and slope factor $q=3$. Figure on left is the $|A_{x_{\mathrm{sp}},x_{\mathrm{sp}}}[k,l]|$ supported on twisted lattice Λ_{q} (lattice points marked in white). Figure on right is $|A_{\tilde{y}^{(0)},x_{\mathrm{sp}}}[k,l]/\sqrt{E_{\mathrm{p}}}|$ and effective channel can be read-off from $A_{\tilde{y}^{(0)},x_{\mathrm{sp}}}[k,l]$ as long as the spread around the lattice point $(0,0)$ is confined within the red rectangle and does not interfere with spread around another lattice point $(k_i,l_i)\neq(0,0)$.

where $(2q)^{-1}$is the unique inverse of $2q$ modulo MN. Thus, $A_{x_{\mathrm{sp}},x_{\mathrm{sp}}}[k,l]=\sum_{(k_i,l_i)\in\Lambda_{\mathrm{q}}} e^{j\theta_i}\delta(k-k_i)\delta(l-l_i)$, where $e^{j\theta_i}$ is the phase associated with the peak at location (k_i,l_i). Note that $A_{x_{\mathrm{sp}},x_{\mathrm{sp}}}[0,0]=\sum_{k=0}^{M-1}\sum_{l=0}^{N-1}|x_{\mathrm{sp}}[k,l]|^2=1$. Substituting $A_{x_{\mathrm{sp}},x_{\mathrm{sp}}}[k,l]$ in (12), we obtain

$$\begin{aligned} A_{\tilde{y}_{\mathrm{sp}}^{(q')},x_{\mathrm{sp}}}[k,l] &= \sum_{(k_i,l_i)\in\Lambda_{\mathrm{q}}} \tilde{h}^{(q')}[k,l] *_\sigma e^{j\theta_i}\delta(k-k_i)\delta(l-l_i) \\ &= \tilde{h}^{(q')}[k,l] + \sum_{(k_i,l_i)\in\Lambda_{\mathrm{q}},(k_i,l_i)\neq(0,0)} e^{j\theta_i}\tilde{h}^{(q')}[k-k_i,l-l_i]e^{j2\pi\frac{k_i(l-l_i)}{MN}}. \end{aligned} \tag{14}$$

In the above equation, the first term corresponds to the effective channel that we are interested in estimating (obtained for $(k_i,l_i)=(0,0)$). The other terms correspond to its repetitions on Λ_{q}. As long as the support of $\tilde{h}^{(q')}[k,l]$ is such that its spread around lattice points in Λ_{q} does not interfere, the effective channel estimate can be obtained using (11), $k\in\{-\lfloor\frac{M}{2}\rfloor, -\lfloor\frac{M}{2}\rfloor+1,\cdots,\lfloor\frac{M}{2}\rfloor\}, l\in\{-\lfloor\frac{N}{2}\rfloor,-\lfloor\frac{N}{2}\rfloor+1,\cdots,\lfloor\frac{N}{2}\rfloor\}$.

Channel estimation in the presence of data: Now, consider the case where the superimposed signal in (2) is transmitted. The estimate of $\tilde{h}^{(q')}[k,l]$ is given by the cross-ambiguity between the received signal in (8) and the transmitted spread pilot signal, i.e.,

$$\begin{aligned} \hat{\tilde{h}}^{(q')}[k,l] &= A_{\tilde{y}^{(q')},x_{\mathrm{sp}}}[k,l]/\sqrt{E_{\mathrm{p}}} \\ &= \tilde{h}^{(q')}[k,l] + \underbrace{\sum_{(k_i,l_i)\in\Lambda_{\mathrm{q}},(k_i,l_i)\neq(0,0)} e^{j\theta_i}\tilde{h}^{(q')}[k-k_i,l-l_i]e^{j2\pi\frac{k_i(l-l_i)}{MN}}}_{\text{Interference due to repetition on }\Lambda_{\mathrm{q}}} \\ &\quad + \underbrace{\sqrt{\frac{E_{\mathrm{d}}}{E_{\mathrm{p}}}}\tilde{h}^{(q')}[k,l] *_\sigma A_{x_{\mathrm{d}},x_{\mathrm{sp}}}}_{\text{Interference from data}} + \underbrace{\frac{A_{n^{(q')},x_{\mathrm{sp}}}}{\sqrt{E_{\mathrm{p}}}}}_{\text{Noise interference}}, \end{aligned} \tag{15}$$

where $\tilde{y}^{(q')}=y^{(q')}e^{-j2\pi\frac{q_\nu k}{MNQ_\nu}}$. In Fig. 3, heatmap of the magnitude of $A_{x_{\mathrm{sp}},x_{\mathrm{sp}}}[k,l]$ and $A_{\tilde{y}^{(0)},x_{\mathrm{sp}}}[k,l]/\sqrt{E_{\mathrm{p}}}$ are plotted to illustrate the channel estimation using cross-ambiguity. From (15), the estimate of channel on the q'th branch $\hat{\mathbf{H}}^{(q')}$ is obtained using $\hat{h}_{\mathrm{dd}}\left(\left(k'+\frac{q_\tau}{Q_\tau}\right)\Delta\tau, \left(l'+\frac{q_\nu}{Q_\nu}\right)\Delta\nu\right)=\hat{\tilde{h}}^{(q')}[k,l]e^{j2\pi\frac{q_\nu k'}{MNQ_\nu}}$ in (10), which is used for channel equalization as described below.

B. Pilot interference cancellation and symbol detection

The estimated pilot interference is canceled from the received signal for symbol detection as

$$\check{\mathbf{y}}^{(q')}=\mathbf{y}^{(q')}-\hat{\mathbf{H}}^{(q')}\mathbf{x}_{\mathrm{sp}}, \tag{16}$$

where $\mathbf{x}_{\mathrm{sp}}[kN+l]=x_{\mathrm{sp}}[k,l]$. For symbol detection, LMMSE equalization is performed on $\{\check{\mathbf{y}}^{(q')}\}_{q'=0}^{Q_\tau Q_\nu-1}$. Let $\{\mathbf{y}_{\mathrm{eq}}^{(q')}\}_{q'=0}^{Q_\tau Q_\nu-1}$ denote the equalized signal on the parallel branches. For each equalized symbol on the q'th branch, $\mathbf{y}_{\mathrm{eq}}^{(q')}[i], i\in\{0,\cdots,MN-1\}$, the symbol from $\mathbb{A}$ having minimum Euclidean distance from $\tilde{\mathbf{y}}_{\mathrm{eq}}^{(q')}[i]$ and the corresponding minimum distance are given by $\mathbf{e}^{(q')}[i]=\arg\min_{a\in\mathbb{A}}\{|\mathbf{y}_{\mathrm{eq}}^{(q')}[i]-a|\}$ and $\mathbf{d}^{(q')}[i]=\min_{a\in\mathbb{A}}\{|\mathbf{y}_{\mathrm{eq}}^{(q')}[i]-a|\}$, respectively. Using $\{\mathbf{d}^{(q')}\}_{q'=0}^{Q_\tau Q_\nu-1}$, $\tilde{q}$ is obtained as $\tilde{q}=\arg\min_{q'=0,\cdots,Q_\tau Q_\nu-1}\mathbf{d}^{(q')}[i]$, and the ith symbol in the frame is detected as $\hat{\mathbf{x}}_{\mathrm{d}}[i]=\mathbf{e}^{(\tilde{q})}[i]$.

C. Turbo iterations

Sections IV-A and IV-B together constitute one complete cycle of channel estimation and data detection. The initial channel estimate in section IV-A is obtained in the presence of interference from data. However, using the detected data in section IV-B to remove its contribution in the received signal and then estimating the channel again could improve performance. This is the motivation behind turbo iterations. This is done as described next. The estimated data contribution on q'th branch is computed as

$$\overline{\mathbf{y}}^{(q')}=\hat{\mathbf{H}}^{(q')}\hat{\mathbf{x}}_{\mathrm{d}}, \tag{17}$$

and subtracted from the received frame to obtain

$$\ddot{\mathbf{y}}^{(q')}=\mathbf{y}^{(q')}-\overline{\mathbf{y}}^{(q')}. \tag{18}$$

The resulting $\{\ddot{\mathbf{y}}^{(q')}\}_{q'=1}^{Q_\tau Q_\nu-1}$ is then used as input to section IV-A. This is repeated N_{iter} number of times. $N_{\mathrm{iter}}=0$ corresponds to case of no turbo iterations.

V. Results and Discussions

In this section, we present the channel estimation and detection performance of the proposed PBS receiver in the superimposed spread pilot framework. The channel estimation performance is measured in terms of normalized mean square error (NMSE) defined as $\mathrm{NMSE}=\frac{1}{Q_\tau Q_\nu}\sum_{q'=0}^{Q_\tau Q_\nu-1}\frac{||\mathbf{H}^{(q')}-\hat{\mathbf{H}}^{(q')}||^2}{||\mathbf{H}^{(q')}||^2}$ and the detection performance is measured in terms of bit error

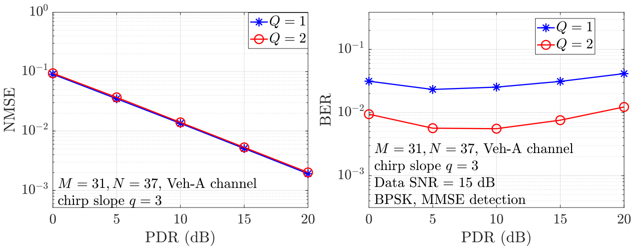

(a) NMSE vs PDR (b) BER vs PDR

Fig. 4: NMSE and BER performance of the proposed PBS receiver as a function of PDR.

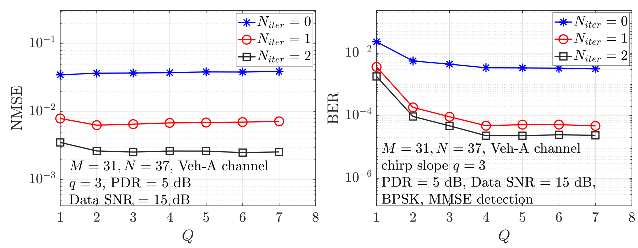

(a) NMSE vs Q (b) BER vs Q

Fig. 5: NMSE and BER performance of the proposed PBS receiver as a function of over-sampling factor Q.

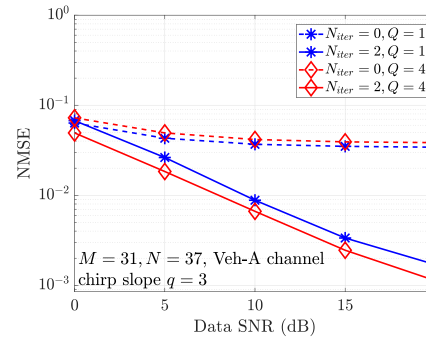

Fig. 6: NMSE performance of the proposed PBS receiver as a function of data SNR.

rate (BER). For this, we consider the following system parameters: $M=31, N=37$, $\nu_p=30$ kHz, $\tau_p=1/\nu_p=3.334$ μs, $B \approx M\nu_p = 930$ KHz, $T \approx N\tau_p = 1.233$ ms, and BPSK. We consider vehicular A (Veh-A) fractional DD channel model [5] with $P=6$, $\tau_{\max}=2.51\mu$s, and $\nu_{\max}=815$ Hz. The path Dopplers are distributed as $\nu_i=\nu_{\max}\cos(\theta)$, $\theta \in \text{Unif}[-\pi,\pi]$. For channel estimation, the point pilot is located at $(k_\text{p}, l_\text{p})=(0,0)$ and the chirp filter slope parameter is $q=3$. Gaussian-sinc filter [12] is chosen as the transmit filter $w_{\text{tx}}(\tau,\nu)$. We consider $Q_\tau=Q_\nu=Q$ in all simulations.

A. NMSE/BER performance as a function of PDR

In Figs. 4a and 4b, we show the NMSE and BER performance, respectively, of the proposed PBS receiver as a function of PDR for conventional sampling ($Q=1$) and over-sampling with a factor of $Q=2$ at a fixed data SNR of 15 dB. From Fig. 4a, it can be seen that the NMSE improves with increasing PDR as expected. However, both $Q=1$ and $Q=2$ show similar NMSE performance because the additional samples due to over-sampling aid the estimation of the additional taps in the effective channel due to over-sampling and do not help to improve the estimates corresponding to the taps on Λ_{dd}. Figure 4b shows that, as the PDR increases, the BER performance initially improves up to a PDR of 5 dB, and starts to degrade for PDRs greater than 5 dB, which can be explained as follows. A low PDR implies low pilot power, leading to a degraded NMSE performance, which, in turn, leads to a degraded detection performance. On the other hand, a high PDR implies high pilot power leading to improved NMSE performance but degraded BER performance due to increased pilot interference to data. Further, it can be observed that the BER performance improves substantially for $Q=2$ compared to that for $Q=1$, indicating the positive influence of over-sampling on the equalization/detection performance. For all simulations in the following, a PDR of 5 dB is used.

B. NMSE/BER as a function of over-sampling factor

Figures 5a and 5b show the NMSE and BER performance, respectively, as a function of over-sampling factor Q for different number of turbo iterations (N_{iter}). In Fig. 5a, it is observed that though the NMSE performance remains almost the same for different values of Q, it improves substantially with turbo iterations due to the effective cancellation of data interference, indicating the positive influence of turbo iterations on the estimation performance. Figure 5b shows that both over-sampling and turbo iterations lead to improved detection performance. In addition, it is observed that the gain due to over-sampling improves drastically with turbo iterations, thus emphasizing the benefits of performing both over-sampling and turbo iterations. It is further observed that the performance gains are marginal for $Q>4$ and $N_{\text{iter}}>2$. We use $Q=4$ and $N_{\text{iter}}=2$ for the simulations that follow.

C. NMSE/BER performance as a function of data SNR

Figures 6 and 7 show the NMSE and BER performance, respectively, as a function of data SNR for $Q=1,4$ and $N_{\text{iter}}=0,2$. In Fig. 6, it is observed that although increasing Q from 1 to 4 leads to only a marginal improvement in NMSE, increasing N_{iter} from 0 to 2 leads to a substantial improvement in NMSE, in line with the observations made earlier. In Fig. 7, it is observed that increasing Q from 1 to 4 improves the BER performance as observed earlier. In addition, incorporating turbo iterations leads to achieving significant improvement, resulting in a BER performance close to that with perfect channel state information (CSI).

VI. Conclusion

In this work, we considered the superimposed spread pilot framework in Zak-OTFS and addressed the problem of channel estimation and detection. We investigated the value of over-sampling in improving channel estimation and detection performance in this framework. In order to mitigate

$$
\begin{aligned}
\hat{\tilde{h}}^{(q')}[k,l] &= \underset{\tilde{h}^{(q')}[k,l]}{\arg\min} \sum_{k=0}^{M-1}\sum_{l=0}^{N-1} -2\mathrm{Re}\Big\{ y_{\mathrm{sp}}^{(q')}[k,l] e^{-j2\pi \frac{q_\nu k}{MNQ_\nu}} \left(\tilde{h}^{(q')}[k,l] *_{\sigma} x_{\mathrm{sp}}[k,l]\right)^{*} \Big\} + \underbrace{\sum_{k=0}^{M-1}\sum_{l=0}^{N-1} \left|\tilde{h}^{(q')}[k,l] *_{\sigma \mathrm{d}} x_{\mathrm{sp}}[k,l]\right|^{2}}_{\mathcal{A}[k,l]} \\
&= \sum_{k'=0}^{M-1}\sum_{l'=0}^{N-1} y_{\mathrm{sp}}^{(q')}[k,l] x_{\mathrm{sp}}^{*}[k-k',l-l'] e^{-j2\pi \frac{(k-k')l'}{MN}} e^{-j2\pi \frac{q_\nu k}{MNQ_\nu}}. \qquad (19)
\end{aligned}
$$

$$
\begin{aligned}
\mathcal{A}[k,l] &= \sum_{k_1',l_1',k_2',l_2' \in \mathbb{Z}} \tilde{h}^{(q')*}[k_1',l_1'] \tilde{h}^{(q')}[k_2',l_2'] \sum_{k=0}^{M-1}\sum_{l=0}^{N-1} x_{\mathrm{sp}}^{*}[k-k_1',l-l_1'] x_{\mathrm{sp}}[k-k_2',l-l_2'] e^{-j2\pi \frac{(k-k_1')l_1'}{MN}} e^{j2\pi \frac{(k-k_2')l_2'}{MN}} \\
&= \sum_{k_1',l_1',k_2',l_2' \in \mathbb{Z}} \tilde{h}^{(q')*}[k_1',l_1'] \tilde{h}^{(q')}[k_2',l_2'] e^{j2\pi \frac{(k_1'-k_2')l_2'}{MN}} A_{x_{\mathrm{s}},x_{\mathrm{s}}}[k_1'-k_2',l_1',l_2'] \\
&\overset{(a)}{=} \sum_{k_1',l_1' \in \mathbb{Z}} \left|\tilde{h}^{(q')}[k_1',l_1']\right|^{2}. \qquad (20)
\end{aligned}
$$

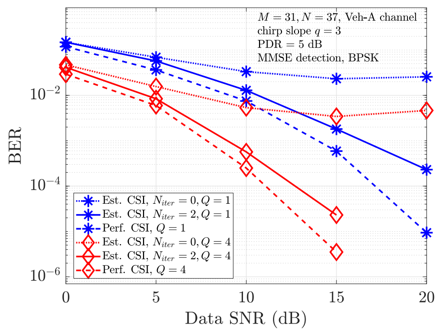

Fig. 7: BER performance of the proposed PBS receiver as a function of data SNR.

the computational complexity incurred due to direct over-sampling, we proposed a parallel branch sampling architecture. In addition, to mitigate pilot-data interference caused by the superposition of pilot and data, turbo iterations between channel estimation and detection were employed. For obtaining the estimate of the effective channel, maximum likelihood estimation was considered and a selection combining based algorithm was proposed for symbol detection. It was observed that while over-sampling provided improved detection performance, turbo iterations helped in improving the channel estimation performance. Together, they achieved close to perfect CSI performance. The current study can be extended to multiuser and MIMO settings as future work.

Appendix A
ML estimate of effective channel on q'th branch

Expanding the optimization problem in (11) and solving, we obtain (19) given at the top of this page. Note that $\left|y_{\mathrm{sp}}^{(q')}[k,l]\right|^2$ is ignored as it is independent of $\tilde{h}^{(q')}[k,l]$. In solving (20), step (a) follows from the fact that $A_{x_{\mathrm{s}},x_{\mathrm{s}}}[k_1'-k_2',l_1'-l_2'] = 0 \ \forall \ k_1' \neq k_2'$ and $l_1' \neq l_2'$ [7].

Appendix B
Derivation of $A_{\tilde{y}_{\mathrm{sp}}^{(q')},x_{\mathrm{sp}}}[k,l]$

Using the definition of cross-ambiguity function, we write

$$
\begin{aligned}
A_{\tilde{y}_{\mathrm{sp}}^{(q')},x_{\mathrm{sp}}}[k,l] = & \sum_{k'=0}^{M-1}\sum_{l'=0}^{N-1} \tilde{y}_{\mathrm{sp}}^{(q')}[k',l'] x_{\mathrm{sp}}^{*}[k'-k,l'-l] \\
& e^{-j2\pi \frac{(k'-k)l}{MN}} \\
\overset{(a)}{=} & \sum_{k'=0}^{M-1}\sum_{l'=0}^{N-1} \left(\tilde{h}^{(q')}[k',l'] *_{\sigma \mathrm{d}} x_{\mathrm{sp}}[k',l']\right) \\
& x_{\mathrm{sp}}^{*}[k'-k,l'-l] e^{-j2\pi \frac{(k'-k)l}{MN}} \\
\overset{(b)}{=} & \tilde{h}^{(q')}[k,l] *_{\sigma \mathrm{d}} A_{x_{\mathrm{sp}},x_{\mathrm{sp}}}[k,l], \qquad (21)
\end{aligned}
$$

where step (a) follows from substituting $\tilde{y}_{\mathrm{sp}}^{(q')}[k,l] = y_{\mathrm{sp}}^{(q')}[k,l] e^{-j2\pi \frac{q_\nu k}{MNQ_\nu}}$, and step (b) follows by using definition of discrete twisted convolution and cross-ambiguity function.

References

[1] R. Hadani et al., "Orthogonal time frequency space modulation," *Proc. IEEE WCNC'2017*, pp. 1-6, Mar. 2017.

[2] Z. Wei et al., "Orthogonal time-frequency space modulation: a promising next-generation waveform," *IEEE Wireless Commun. Mag.*, vol. 28, no. 4, pp. 136-144, Aug. 2021.

[3] A. J. E. M. Janssen, "The Zak transform: a signal transform for sampled time-continuous signals," *Philips J. Res.*, 43, pp. 23-69, 1988.

[4] S. K. Mohammed et al., "OTFS — a mathematical foundation for communication and radar sensing in the delay-Doppler domain," *IEEE BITS the Inform. Theory Mag.*, vol. 2, no. 2, pp. 36-55, Nov. 2022.

[5] S. K. Mohammed et al., "OTFS — predictability in the delay-Doppler domain and its value to communication and radar sensing," *IEEE BITS the Inform. Theory Mag.*, vol. 3, no. 2, pp. 7-31, Jun. 2023.

[6] S. K. Mohammed, R. Hadani, and A. Chockalingam, *OTFS Modulation — Theory and Applications*, IEEE-Wiley, 2024.

[7] Muhammad Ubadah et al., "Zak-OTFS to integrate sensing the I/O relation and data communication," *arXiv:2404.04182 [eess.SP]*.

[8] S. Gopalam, H. Inaltekin, I. B. Collings, and S. V. Hanly, "Optimal Zak-OTFS receiver and its relation to the radar matched filter," *IEEE Open J. of the Commun. Soc.*, vol. 5, pp. 4462-4482, 2024.

[9] Y. Ge, Q. Deng, P. C. Ching and Z. Ding, "Receiver design for OTFS with a fractionally spaced sampling approach", *IEEE Trans. Wireless Commun.*, vol. 20, no. 7, pp. 4072-4086, July 2021.

[10] P. Priya, E. Viterbo and Y. Hong, "Low complexity MRC detection for OTFS receiver with oversampling," *IEEE Trans. Wireless Commun.*, vol. 23, no. 2, pp. 1459-1473, Feb. 2024.

[11] N. Deconda, N. Seshadri, R. D. Koilpillai, "A modified MRC receiver for OTFS systems with oversampling," *IEEE WCNC'2024*, Apr. 2024.

[12] A. Das, F. Jesbin, and A. Chockalingam, "A Gaussian-sinc pulse shaping filter for Zak-OTFS," *IEEE Trans. Veh. Tech.*, Feb. 2025, doi: 10.1109/TVT.2025.3609781.